Electronic Supplementary Information

$[RbSr_3X][(BS_3)_2]$ (X = Cl, Br): Two salt-inclusion thioborates with large birefringence and structure transformation from centrosymmetric to asymmetric †

Yihan Yun,[a, b] Xueling Hou,[a, b] Zhihua Yang,[a, b] Guangmao Li,[*a, b] and Shilie Pan[*a, b]

†Research Center for Crystal Materials; CAS Key Laboratory of Functional Materials and Devices for Special Environments; Xinjiang Technical Institute of Physics & Chemistry, CAS, 40-1 South Beijing Road, Urumqi 830011, China.

‡Center of Materials Science and Optoelectronics Engineering, University of Chinese Academy of Sciences, Beijing 100049, China.

**Corresponding authors' e-mails: slpan@ms.xjb.ac.cn; ligm@ms.xjb.ac.cn*

† Electronic supplementary information (ESI) available: Experimental and calculation details, related figures, tables and crystal data. CCDC 2299855 for $[RbSr_3Cl][(BS_3)_2]$ and 2299856 for $[RbSr_3Br][(BS_3)_2]$. For ESI and crystallographic data in CIF or other electronic format see DOI:xxx

Experimental Section

Synthesis of $[RbSr_3X][(BS_3)_2]$ (X = Cl, Br).

(1) The crystals of $[RbSr_3Cl][(BS_3)_2]$ for single crystal X-ray diffraction were obtained by spontaneous crystallization method. The synthesis processes are as follows: 1) A mixture of RbCl (0.151 g), SrS (0.150 g), B (0.014 g) and S (0.080 g) was mixed in an agate mortar, which was placed in the graphite crucible. 2) The crucible was covered with a tight crucible cap and then moved into a glassy carbon-inwall coated silica tube. 3) The crucible was sealed by oxyhydrogen flame under a vacuumed environment (10^{-4} Pa). 4) After that, the sealed tube was put into a temperature program-controlled furnace with the heating progress as follow:

30 ºC (50 ºC/h) → 180 ºC (keep for 5 h) (64 ºC/h) → 500 ºC (keep for 5 h) (60 ºC/h) → 800 ºC (keep for 33 h) (9 ºC/h) → 500 ºC (94 ºC/h) → 30 ºC.

(2) The crystals of $[RbSr_3Br][(BS_3)_2]$ for single crystal X-ray diffraction were obtained by spontaneous crystallization method. The synthesis process and heating progress are similar to that of $[RbSr_3Cl][(BS_3)_2]$.

Single X-ray diffraction measurement and structure refinement. The structure data of $[RbSr_3X][(BS_3)_2]$ (X = Cl, Br) were collected on a Bruker SMART APEX II 4K CCD diffractometer equipped with Mo Kα radiation (λ = 0.71073 Å) operating at 50 kV and 40 mA at room temperature. The data were refined through full-matrix least-squares on F^2 using SHELXTL program package.[1] Structure determination was based on the direct method, and the face-indexed absorption correction was made with XPREP Program. The final structure was checked with PLATON and no higher symmetries were found. During the analysis process, it was found that the Flack was too large and the *R* value was too high and Platon detected inverted twins, the matrix was (-1,0,0,0,1,0,0,0,-1). By adding twin instructions, the *R* value was decreased to a reasonable level and Flack decreased to 0.02. Owing to the twinning treatment and HKLF5 splitting treatment, the R_{int} value is meaningless.

Powder X-ray diffraction measurement. X−ray diffraction (XRD) characterization for $[RbSr_3X][(BS_3)_2]$ (X = Cl, Br) was implemented on an automated Bruker D2 X-ray diffractometer from 10 to 70 ° (2θ) with a scan step width of 0.02 ° and a fixed counting time of 1 s/step.

Rapid temperature rise and fall experiment. A mixture of RbX (X = Cl, Br), SrS, B and S was mixed in an agate mortar according to stoichiometric ratio, which was placed in the graphite crucible. The crucible was covered with a tight crucible cap and then moved into a glassy carbon-inwall coated silica tube. Then, the silica tube was sealed by oxyhydrogen flame under a vacuumed environment (10^{-4} Pa). After that, the sealed tube was put into a temperature program-controlled furnace with the heating progress set as: rising from room temperature to 900 °C within ten hours and then dropping to room temperature within ten hours.

Energy dispersive X-ray spectroscopy. Elemental analysis was carried on clean single crystal surfaces with the aid of a field emission scanning electron microscope (SEM, SUPRA 55VP) equipped with an energy dispersive X-ray spectroscope (EDX, BRUKER x-flash-sdd-5010).

Raman spectroscopy. To investigate the Raman spectra of $[RbSr_3X][(BS_3)_2]$ (X = Cl, Br), a LABRAM HR Evolution spectrometer equipped with a CCD detector by a 633 nm radiation was used to record Raman scattering spectroscopy data in the 1000−100 cm^{-1} region. High-quality single crystals of the title compound were put on a glass slide and located by using a 50 × objective lens for the measurements. The laser with 633 nm radiation was applied for the characterizations, and the maximum power was 60 MW. The radiation kept at this power for 15 s to complete the measurements.

Infrared absorption spectrum. The IR spectrum was recorded on a Shimadzu IR Affinity-1 Fourier transform infrared spectrometer with a resolution of 2 cm^{-1}, covering the wavenumber range of 400-4000 cm^{-1}. The crystal samples and KBr were mixed in the ratio of about 1:100, dried, and ground into fine powder and then pressed into a transparent sheet on the tablet machine. The sheet was loaded in the sample chamber, and then the IR absorption spectrum was measured.

UV–vis–NIR diffuse reflectance spectroscopy. Optical diffuse reflectance spectra of $[RbSr_3X][(BS_3)_2]$ (X = Cl, Br) was measured at 298 K on Shimadzu SolidSpec-3700DUV spectrophotometer with a wavelength range of 190–2600 nm, which can provide the visible or UV cut-off edge. The experimental band gaps of $[RbSr_3X][(BS_3)_2]$ (X = Cl, Br) can be estimated by converting the reflectance spectra to absorbance using Kubelka-Munk function.[2]

Birefringence measurement. The birefringence of $[RbSr_3X][(BS_3)_2]$ (X = Cl, Br) was characterized by using the polarizing microscope equipped (ZEISS Axio Scope. A1) with Berek compensator.[3-5] The wavelength of the light source was 546 nm. The difference in the optical path (R) for one direction was determined according to the interference color with the maximum value of the crystal under the polarized light.

The formula for calculating the birefringence is listed below,

$R = |N_2 - N_1| \times T = \Delta n \times T$.

Herein, Δn means the difference of refractive index, and T denotes the thickness of the crystal.

Powder laser-induced damage threshold measurement. On the same measurement condition, the LIDT of $[RbSr_3X][(BS_3)_2]$ (X = Cl, Br) was evaluated by a single-pulse measurement method, with $AgGaS_2$ as the reference. The samples of $[RbSr_3X][(BS_3)_2]$ (X = Cl, Br) and $AgGaS_2$ were finely ground and sieved, among which samples with a particle size among 45-63 μm were collected and pressed into the sample trays. The samples were exposed to a pulsed laser beam (2.09 μm, 50 ns, 3 Hz) while the pulse energy was continuously increased. Energy increase was stopped when a damage occurrence (color change) was detected on the sample surface under a microscope.

Second-harmonic generation. The SHG response of $[RbSr_3Br][(BS_3)_2]$ was measured through the Kurtz−Perry method with a 2.09 μm Q-switch laser.[6] The $[RbSr_3Br][(BS_3)_2]$ samples were ground and sieved into different particle sizes: 45−63, 63−90, 90−125, 125−180, and 180−212 μm. These samples were placed between two glass microscope slides and fixed with a 1 mm-thick, 8 mm-diameter silicone. Then, they were placed into a Q-switched Ho:Tm:Cr:YAG laser with a wavelength of 2.09 μm, and the SHG signals were recorded by an oscilloscope connected to the laser. The $AgGaS_2$ samples with the same particle sizes were used as the references.

First-principles calculations. The theoretical calculations were implemented in the CASTEP using a planewave pseudopotential method based on density function theory[7] to obtain the electronic structures and optical properties for $[RbSr_3X][(BS_3)_2]$ (X = Cl, Br) and $Sr_3B_2S_6$. The generalized gradient approximation (GGA)[8] was adopted, and the Perdew-Burke-Ernzerhof (PBE) functional[9] was chosen to describe the exchange-correlation energy, with the energy cutoff of 750 and 650 eV, respectively. The *k*-point separation for each material was set as 0.035 $Å^{-1}$ in the Brillouin zone. Norm-conserving pseudopotentials (NCP)[10] were employed for each atomic species with the following valence configurations: Rb-$4s^2 4p^6 5s^1$, Sr-$4s^2 4p^6 5s^2$, B-$2s^2 2p^1$, S-$3s^2 3p^4$, Cl-$3s^2 3p^5$, Br-$4s^2 4p^5$. Other calculation parameters and convergent criteria were set as the default values of the CASTEP package.[11] For $[RbSr_3X][(BS_3)_2]$ (X = Cl, Br), the bandgap difference between the experimental values and the values calculated by GGA method was used as the scissors operation to calculate the birefringence and the SHG coefficients. The corresponding values of scissors operation were set as 1.04 and 1.15 eV. For $Sr_3B_2S_6$, the Heyd-Scuseria-Ernzerhof (HSE06) hybrid functional[12] was adopted for more accurate band gap values since there was no experimental band gap. The bandgap difference between the HSE value and the value calculated by GGA method was used as the scissors operation to calculate the birefringence. The corresponding value of scissors operation were set as 0.98 eV. The Gaussian 09 package was employed to explore the NLO-related effect of thioborates anionic groups, including $[BS_3]$, $[BS_4]$, $[BO_3]$, $[BO_4]$ and $[GaS_4]$ groups. B3LYP (Becke, three-parameter, Lee-Yang-Parr) exchange-correlation functional with the Lee-Yang-Parr correlation functional at the 6-31G basis set was adopted.

Calculation methods for optical properties. The calculations of the linear optical performance were described in terms of the complex dielectric constant $\varepsilon(\omega) = \varepsilon_1(\omega) + i\varepsilon_2(\omega)$. The imaginary part $\varepsilon_2(\omega)$ of the dielectric function $\varepsilon(\omega)$ was calculated by using momentum matrix elements between the occupied and unoccupied electronic states:

$$\varepsilon_2(\hbar\omega) = \frac{2e^2\pi}{\Omega\varepsilon_0}\sum_{kcv}\left|\langle\psi_k^c|\hat{u}\cdot r|\psi_k^v\rangle\right|^2\delta\left[E_k^c - E_k^v - E\right]$$

Here Ω is the unit cell volume, v and c represent the valence bands and conduction bands, respectively. ω and $\hat{u}$ are the frequency and the unit vector in the polarization direction of the incident light. Under the periodic boundary condition, $|\langle\psi_k^c|\hat{u}\cdot r|\psi_k^v\rangle|$ is the transition matrix element between the valence bands and the conduction bands at a specific k point in the first Brillouin zone. The real part $\varepsilon_1(\omega)$ can be obtained from the imaginary part $\varepsilon_2(\omega)$ by using the Kramers-Kronig transformation. The refractive index *n* and birefringence Δn can be obtained from the complex dielectric function.[13] Furthermore, the response electron distribution anisotropy (REDA) method[14] was employed to identify the contribution of each group to birefringence and the birefringence can be estimated as follow:

$$\Delta n = \frac{\Re\sum_g\left[N_c Z_a \Delta\rho^b\right]_g}{2n_1 E_o}$$

Here, $\Re$ is the correction coefficient, N_c is the coordination number of the nearest

neighbor cations to the central anion, Z_a is the formal chemical valence of the anion, $\Delta\rho^b$ is the difference between the maximum and minimum of the covalent electron density of the covalent bond on the optical principal axes of a crystal, E_o is the optical bandgap, n_1 is the minimum refractive index. The second-order susceptibility $\chi^{(2)}$ tensors are calculated by the so-called length-gauge formalism derived by Sipe and developed by Lin et al. At a zero frequency, the static second-order nonlinear susceptibilities can be described to virtual electrons (VE) and virtual hole (VH) processes. As shown below:

$$\chi^{(2)}_{\alpha\beta\gamma} = \chi^{(2)}_{\alpha\beta\gamma}(\mathrm{VE}) + \chi^{(2)}_{\alpha\beta\gamma}(\mathrm{VH})$$

Where $\chi^{(2)}_{\alpha\beta\gamma}(\mathrm{VE})$ and $\chi^{(2)}_{\alpha\beta\gamma}(\mathrm{VH})$ are computed with the formulas as follows:

$$\chi_{\alpha\beta\gamma}{}^{(2)}(\mathrm{VE}) = \frac{e^3}{2\hbar^2 m^3}\sum_{vcc'}\int\frac{d^3k}{4\pi^3}P(\alpha\beta\gamma)\,\mathrm{Im}\left[p^{\alpha}_{cv}p^{\beta}_{cc'}p^{\gamma}_{c'v}\right] \times\left(\frac{1}{\omega^3_{cv}\omega^2_{vc'}}+\frac{2}{\omega^4_{vc}\omega_{c'v}}\right)$$

$$\chi_{\alpha\beta\gamma}{}^{(2)}(\mathrm{VH}) = \frac{e^3}{2\hbar^2 m^3}\sum_{vv'c}\int\frac{d^3k}{4\pi^3}P(\alpha\beta\gamma)\,\mathrm{Im}\left[p^{\alpha}_{vv'}p^{\beta}_{cv'}p^{\gamma}_{cv}\right] \times\left(\frac{1}{\omega^3_{cv}\omega^2_{v'c}}+\frac{2}{\omega^4_{vc}\omega_{cv'}}\right)$$

Here, α, β, and γ are the Cartesian components; v/v' and c/c' denote the valence bands and conduction bands; $P(\alpha\beta\gamma)$, $\hbar\omega_{ij}$, and p^{α}_{ij} refer to the full permutation, band energy difference, and momentum matrix elements, respectively.

Table S1. Crystal data and structure refinement for $[RbSr_3X][(BS_3)_2]$ (X = Cl, Br).

empirical formula	$[RbSr_3Cl][(BS_3)_2]$	$[RbSr_3Br][(BS_3)_2]$
formula weight	597.76	642.22
temperature	293.00 K	300.00 K
crystal system, space group	orthorhombic, *Pbca*	orthorhombic, $Cmc2_1$
unit cell dimensions	a = 11.0820(4) Å	a = 15.044(4) Å
	b = 7.9064(3) Å	b = 10.9780(3) Å
	c = 29.1239(14) Å	c = 7.8706(19) Å
volume	2551.80(18) Å^3	1299.9(6) Å^3
Z, calculated density	8, 3.112 g/cm^3	4, 3.281 g/cm^3
absorption coefficient	17.426 mm^{-1}	19.972 mm^{-1}
F(000)	2192.0	1168.0
2θ range for data collection	4.618 – 55.062 °	4.594 – 55.054 °
limiting indices	$-14 \le h \le 14$, $-10 \le k \le 9$, $-37 \le l \le 37$	$0 \le h \le 19$, $0 \le k \le 14$, $-10 \le l \le 10$
reflections collected/unique	19247/2926[R(int) = 0.0702]	1491/1491[R(int) = N/A[b]]
refinement method	full-matrix least-squares on F^2	full-matrix least-squares on F^2
data/restraints/parameters	2926/0/119	1491/1/65
goodness-of-fit on F^2	1.051	1.207
final R indices [$I > 2\sigma(I)$][a]	R_1 = 0.0375, wR_2 = 0.0867	R_1 = 0.0222, wR_2 = 0.0513
R indices (all data)[a]	R_1 = 0.0541, wR_2 = 0.0952	R_1 = 0.0223, wR_2 = 0.0514
largest diff. peak and hole	1.91 and −1.43 e·Å^{-3}	1.41 and −1.42 e·Å^{-3}
flack parameter	N/A[b]	0.017 (3)

[a] $R_1 = \Sigma||F_o| - |F_c||/\Sigma|F_o|$ and $wR_2 = [\Sigma w(F_o^2 - F_c^2)^2/\Sigma wF_o^4]^{1/2}$ for $F_o^2 > 2\sigma(F_o^2)$

[b] N/A=not available

Table S2. The atomic coordinates, equivalent isotropic displacement parameters and BVS in $[RbSr_3Cl][(BS_3)_2]$.

Atom	x	y	z	U(eq)	BVS
Rb1	1302.2(7)	8156.2(11)	6222.9(2)	48.8(2)	0.99
Sr1	4503.1(5)	7703.2(6)	5219.6(2)	18.83(15)	2.05
Sr2	4474.5(5)	7355.9(6)	7278.8(2)	18.74(15)	2.05
Sr3	2872.1(5)	2365.4(6)	8736.3(2)	19.80(14)	1.89
B1	2234(5)	5094(7)	7771(2)	16.8(11)	3.04
B2	2429(5)	5245(7)	4706(2)	19.3(12)	3.03
S1	3715.2(11)	4970.8(16)	8041.7(5)	19.5(3)	2.05
S2	958.8(12)	4523.0(16)	8140.4(5)	19.7(3)	2.15
S3	1158.7(12)	4712.4(16)	4337.4(5)	19.3(3)	2.12
S4	3924.7(12)	5163.1(16)	4447.7(5)	20.0(3)	2.02
S5	1989.1(13)	5767.0(18)	7191.1(5)	27.2(3)	1.85
S6	2121.1(14)	5910.0(19)	5288.4(5)	28.6(3)	1.90
Cl1	4209.1(14)	7522.7(17)	6249.3(5)	27.2(3)	0.94

Table S3. The atomic coordinates, equivalent isotropic displacement parameters and BVS in $[RbSr_3Br][(BS_3)_2]$.

Atom	x	y	z	U(eq)	BVS
Rb1	5000	3552.1(7)	2840.7(13)	30.7(2)	1.17
Sr1	10000	5363.1(5)	7699.0(7)	14.39(15)	1.80
Sr2	7101.8(2)	6992.7(3)	2629.4(6)	13.06(13)	1.99
B1	8110(3)	4701(4)	4904(7)	13.0(10)	3.04
S1	8790.7(9)	3388.3(11)	5473.2(15)	14.4(2)	2.08
S2	8657.2(8)	6190.2(10)	5033.8(16)	14.4(2)	2.00
S3	6995.2(8)	4484.3(12)	4167.8(18)	19.7(3)	1.94
Br1	5000	6579.4(6)	2305.8(9)	20.85(19)	0.99

Table S4. Selected bond lengths [Å] for $[RbSr_3Cl][(BS_3)_2]$.

Atom	Atom	Length/Å	Atom	Atom	Length/Å
Rb1	S2[11]	3.2992(15)	Sr2	S2[4]	3.0763(15)
Rb1	Cl1[4]	3.4994(16)	Sr2	Cl1	3.0154(17)
Rb1	Cl1	3.2611(17)	Sr2	S5[6]	3.4247(17)
Rb1	S3[12]	3.9043(16)	Sr2	S5	3.0380(15)
Rb1	S4[13]	3.5387(15)	Sr2	S5[4]	3.1575(14)
Rb1	S5[4]	3.9745(18)	Sr3	S1	3.0345(14)
Rb1	S5	3.4783(16)	Sr3	S1[7]	3.2818(14)
Rb1	S6	3.3740(16)	Sr3	S2	3.2275(14)
Rb1	S6[4]	3.8987(19)	Sr3	S2[7]	3.1209(14)
Sr1	Cl1	3.0199(16)	Sr3	Cl1[8]	3.2372(16)
Sr1	S3[3]	3.0341(14)	Sr3	S3[9]	3.0913(14)
Sr1	S3[4]	3.1087(14)	Sr3	S3[10]	3.0608(14)
Sr1	S4[5]	3.0182(14)	Sr3	S4[9]	3.4752(15)
Sr1	S4	3.0819(14)	Sr3	S4[10]	3.1066(14)
Sr1	S6	3.0031(15)	B1	S1	1.824(6)
Sr1	S6[3]	3.4364(18)	B1	S2	1.833(6)
Sr1	S6[4]	3.1159(15)	B2	S3	1.820(6)
Sr2	S1	3.0333(14)	B2	S4	1.821(6)
Sr2	S1[2]	3.0283(14)	B1	S5	1.791(6)
Sr2	S2[6]	3.0353(14)	B2	S6	1.808(7)

[1]1-X,2-Y,1-Z; [2]1-X,1/2+Y,3/2-Z; [3]1/2+X,3/2-Y,1-Z; [4]1/2-X,1/2+Y,+Z; [5]1-X,1-Y,1-Z; [6]1/2+X,+Y,3/2-Z; [7]1/2-X,-1/2+Y,+Z; [8]1-X,-1/2+Y,3/2-Z; [9]1/2-X,1-Y,1/2+Z; [10]+X,1/2-Y,1/2+Z; [11]-X,1/2+Y,3/2-Z; [12]-X,1-Y,1-Z; [13]-1/2+X,3/2-Y,1-Z

Table S5. Selected bond lengths [Å] for $[RbSr_3Br][(BS_3)_2]$.

Atom	Atom	Length/Å	Atom	Atom	Length/Å
Rb1	$S1^{10}$	3.3645(15)	Sr1	$S2^{4}$	3.0505(14)
Rb1	$S1^{11}$	3.3645(15)	Sr1	$S2^{1}$	3.2196(13)
Rb1	$S2^{12}$	3.7127(16)	Sr2	Br1	3.2045(9)
Rb1	$S2^{13}$	3.7127(16)	Sr2	$S1^{6}$	3.0265(14)
Rb1	S3	3.3389(14)	Sr2	$S1^{7}$	3.0840(15)
Rb1	$S3^{14}$	3.3390(14)	Sr2	$S2^{5}$	3.0752(13)
Sr1	$Br1^{2}$	3.3709(12)	Sr2	S2	3.1358(14)
Sr1	$S1^{3}$	3.1554(14)	Sr2	S3	3.0125(14)
Sr1	S1	3.3285(14)	Sr2	$S3^{6}$	3.2854(16)
Sr1	$S1^{4}$	3.3286(14)	Sr2	$S3^{7}$	3.1746(15)
Sr1	$S1^{1}$	3.1554(14)	B1	S1	1.824(5)
Sr1	S2	3.0505(14)	B1	S2	1.834(5)
Sr1	$S2^{3}$	3.2196(13)	B1	S3	1.790(5)

[1]2-X,1-Y,1/2+Z; [2]3/2-X,3/2-Y,1/2+Z; [3]+X,1-Y,1/2+Z; [4]2-X,+Y,+Z; [5]3/2-X,3/2-Y,-1/2+Z; [6]3/2-X,1/2+Y,+Z; [7]+X,1-Y,-1/2+Z; [8]1-X,1-Y,1/2+Z; [9]1-X,1-Y,-1/2+Z; [10]3/2-X,1/2-Y,-1/2+Z; [11]-1/2+X,1/2-Y,-1/2+Z; [12]-1/2+X,-1/2+Y,+Z; [13]3/2-X,-1/2+Y,+Z; [14]1-X,+Y,+Z

Table S6. Selected bond angles [°] for $[RbSr_3Cl][(BS_3)_2]$.

Atom	Atom	Atom	Angle/°	Atom	Atom	Atom	Angle/°
$S2^{11}$	Rb1	$Cl1^{3}$	62.71(4)	S6	Sr1	Cl1	79.43(4)
$S2^{11}$	Rb1	$S3^{12}$	83.95(4)	S6	Sr1	$S3^{3}$	95.11(4)
$S2^{11}$	Rb1	$S4^{13}$	67.77(4)	S6	Sr1	$S3^{4}$	145.19(4)
$S2^{11}$	Rb1	S5	83.60(4)	S6	Sr1	$S4^{5}$	97.56(4)
$S2^{11}$	Rb1	$S5^{3}$	78.05(4)	S6	Sr1	S4	63.78(4)
$S2^{11}$	Rb1	$S6^{3}$	123.35(4)	S6	Sr1	$S6^{3}$	82.650(18)
$S2^{11}$	Rb1	S6	146.10(4)	$S6^{3}$	Sr1	$S6^{4}$	104.82(4)
Cl1	Rb1	$Cl1^{3}$	108.12(4)	S6	Sr1	$S6^{4}$	157.14(2)
Cl1	Rb1	$S3^{12}$	127.64(4)	$S2^{6}$	Sr2	$S5^{3}$	151.18(4)
$Cl1^{3}$	Rb1	$S3^{12}$	117.98(4)	$S2^{3}$	Sr2	$S5^{3}$	60.67(4)
$Cl1^{3}$	Rb1	$S4^{13}$	61.39(4)	Cl1	Sr2	S1	136.76(4)
Cl1	Rb1	$S4^{13}$	143.73(4)	Cl1	Sr2	$S1^{2}$	74.23(4)
Cl1	Rb1	S5	71.41(4)	Cl1	Sr2	$S2^{6}$	71.65(4)
Cl1	Rb1	$S5^{3}$	65.94(4)	Cl1	Sr2	$S2^{3}$	140.49(4)
$Cl1^{3}$	Rb1	$S5^{3}$	63.20(4)	S1	Sr2	$S5^{6}$	70.58(4)
$Cl1^{3}$	Rb1	$S6^{3}$	62.42(4)	$S2^{6}$	Sr2	$S2^{3}$	145.46(3)
Cl1	Rb1	S6	70.88(4)	$S2^{3}$	Sr2	$S5^{6}$	87.91(4)
Cl1	Rb1	$S6^{3}$	70.10(4)	$S2^{6}$	Sr2	S5	98.76(4)
$S4^{13}$	Rb1	$S6^{3}$	74.85(3)	$S2^{6}$	Sr2	$S5^{6}$	57.97(4)
S5	Rb1	$Cl1^{3}$	123.60(4)	S5	Sr2	$S5^{6}$	128.61(4)
S5	Rb1	$S3^{12}$	100.15(4)	$S5^{3}$	Sr2	$S5^{6}$	140.16(4)
S5	Rb1	$S4^{13}$	144.52(4)	Cl1	Sr2	S5	81.14(4)
S5	Rb1	$S5^{3}$	66.59(3)	Cl1	Sr2	$S5^{6}$	122.93(4)
S5	Rb1	$S6^{3}$	140.45(4)	Cl1	Sr2	$S5^{3}$	80.33(4)
S6	Rb1	Cl13	125.49(4)	S5	Sr2	$S2^{3}$	99.06(4)
S6	Rb1	$S3^{12}$	62.94(3)	S5	Sr2	$S5^{3}$	83.15(2)
$S6^{3}$	Rb1	$S3^{12}$	110.23(3)	S1	Sr3	$S1^{7}$	98.38(4)
S6	Rb1	$S4^{13}$	87.29(4)	S1	Sr3	S2	59.01(3)
S6	Rb1	$S5^{3}$	135.85(4)	S1	Sr3	$S2^{7}$	89.45(4)
S63	Rb1	$S5^{3}$	89.52(4)	S1	Sr3	$Cl1^{8}$	71.03(4)
S6	Rb1	S5	108.01(4)	S1	Sr3	$S3^{9}$	159.49(4)
S6	Rb1	$S6^{3}$	67.07(3)	S1	Sr3	$S3^{10}$	76.30(4)
Cl1	Sr1	$S3^{3}$	145.04(4)	S1	Sr3	$S4^{9}$	139.98(4)
Cl1	Sr1	$S3^{4}$	71.02(4)	S1	Sr3	$S4^{10}$	101.08(3)
Cl1	Sr1	S4	132.15(4)	$S1^{7}$	Sr3	$S4^{10}$	112.63(4)
Cl1	Sr1	$S6^{3}$	84.97(4)	$S2^{7}$	Sr3	$S1^{7}$	57.61(3)
Cl1	Sr1	$S6^{4}$	122.26(4)	$S2^{7}$	Sr3	S2	110.76(5)
$S3^{4}$	Sr1	$S3^{3}$	98.63(4)	S2	Sr3	$Cl1^{8}$	130.02(4)
$S3^{4}$	Sr1	S4	151.02(4)	$S2^{7}$	Sr3	$Cl1^{8}$	67.67(4)
$S3^{4}$	Sr1	$S6^{3}$	76.94(4)	$S2^{7}$	Sr3	$S4^{10}$	166.98(4)
$S3^{3}$	Sr1	$S6^{3}$	60.07(4)	S2	Sr3	$S4^{10}$	69.33(3)

Cl1[8]	Sr3	S1[7]	124.45(4)	S3[10]	Sr3	S4[9]	88.44(4)
Cl1[8]	Sr3	S4[10]	122.90(4)	S2	Sr3	S1[7]	67.75(3)
S3[10]	Sr3	S1[7]	165.11(4)	S4[9]	Sr3	S1[7]	103.95(4)
S3[9]	Sr3	S1[7]	73.17(4)	S4[9]	Sr3	S2	160.98(4)
S3[9]	Sr3	S2[7]	100.90(4)	S4[9]	Sr3	S2[7]	75.62(4)
S3[10]	Sr3	S2	97.91(4)	S4[9]	Sr3	Cl1[8]	68.96(4)
S3[10]	Sr3	S2[7]	135.14(4)	S4[9]	Sr3	S4[10]	100.33(4)
S3[9]	Sr3	S2	100.58(4)	S1	B1	S2	115.2(3)
S3[9]	Sr3	Cl1[8]	129.28(4)	S5	B1	S1	124.0(3)
S3[10]	Sr3	Cl1[8]	67.47(4)	S5	B1	S2	120.7(3)
S3[9]	Sr3	S3[10]	107.02(5)	S3	B2	S4	116.9(4)
S3[9]	Sr3	S4[9]	60.40(4)	S6	B2	S3	118.3(3)
S3[10]	Sr3	S4[10]	56.03(4)	S6	B2	S4	124.7(4)
S3[9]	Sr3	S4[10]	66.75(4)				

Symmetry transformations used to generate equivalent atoms:

[1]1-X,2-Y,1-Z; [2]1-X,1/2+Y,3/2-Z; [3]1/2-X,1/2+Y,+Z; [4]1/2+X,3/2-Y,1-Z; [5]1-X,1-Y,1-Z; [6]1/2+X,+Y,3/2-Z; [7]1/2-X,-1/2+Y,+Z; [8]1-X,-1/2+Y,3/2-Z; [9]+X,1/2-Y,1/2+Z; [10]1/2-X,1-Y,1/2+Z; [11]-X,1/2+Y,3/2-Z; [12]-X,1-Y,1-Z; [13]-1/2+X,3/2-Y,1-Z; [14]- 1/2+X,+Y,3/2-Z; [15]-X,-1/2+Y,3/2-Z; [16]1/2-X,1-Y,-1/2+Z; [17]+X,1/2-Y,-1/2+Z

Table S7. Selected bond angles [°] for $[RbSr_3Br][(BS_3)_2]$.

Atom	Atom	Atom	Angle/°	Atom	Atom	Atom	Angle/°
Br1	Rb1	$Br1^{9}$	99.57(3)	$S1^{2}$	Sr1	$S2^{2}$	58.22(4)
Br1	Rb1	$S1^{14}$	123.95(4)	$S2^{2}$	Sr1	$Br1^{1}$	125.44(3)
Br1	Rb1	$S1^{11}$	123.95(4)	$S2^{3}$	Sr1	$Br1^{1}$	68.93(3)
Br1	Rb1	$S2^{13}$	138.70(3)	$S2^{4}$	Sr1	$Br1^{1}$	125.44(3)
Br1	Rb1	$S2^{12}$	138.70(3)	S2	Sr1	$Br1^{1}$	68.93(3)
$Br1^{9}$	Rb1	$S2^{12}$	60.45(3)	S2	Sr1	$S1^{4}$	87.98(4)
$Br1^{9}$	Rb1	$S2^{13}$	60.45(3)	$S2^{2}$	Sr1	S1	107.36(4)
$S1^{14}$	Rb1	$Br1^{9}$	121.83(3	$S2^{3}$	Sr1	$S1^{3}$	57.99(4)
$S1^{11}$	Rb1	$Br1^{9}$	121.83(3)	$S2^{3}$	Sr1	$S1^{4}$	136.75(4)
$S1^{14}$	Rb1	$S1^{11}$	65.47(5)	$S2^{3}$	Sr1	S1	101.18(4)
$S1^{14}$	Rb1	$S2^{12}$	61.38(3)	$S2^{4}$	Sr1	$S1^{3}$	107.36(4)
$S1^{14}$	Rb1	$S2^{13}$	96.29(4)	$S2^{3}$	Sr1	$S1^{2}$	87.98(4)
$S1^{11}$	Rb1	$S2^{12}$	96.29(4)	S2	Sr1	S1	57.99(4)
$S1^{11}$	Rb1	$S2^{13}$	61.38(3)	$S2^{2}$	Sr1	$S1^{3}$	67.20(3)
$S2^{12}$	Rb1	$S2^{13}$	65.93(4)	S2	Sr1	$S1^{2}$	136.75(4)
$S3^{10}$	Rb1	Br1	74.65(3)	S2	Sr1	$S1^{3}$	101.18(4)
S3	Rb1	Br1	74.65(3)	$S2^{4}$	Sr1	S1	67.20(3)
S3	Rb1	$Br1^{9}$	72.54(3)	$S2^{3}$	Sr1	$S2^{4}$	164.94(3)
$S3^{10}$	Rb1	$Br1^{9}$	72.54(3)	S2	Sr1	$S2^{4}$	97.74(4)
$S3^{10}$	Rb1	$S1^{14}$	83.18(4)	$S2^{2}$	Sr1	$S2^{4}$	77.72(5)
$S3^{10}$	Rb1	$S1^{11}$	148.59(4)	$S2^{3}$	Sr1	$S2^{2}$	97.74(4)
S3	Rb1	$S1^{14}$	148.59(4)	$S2^{3}$	Sr1	S2	82.94(5)
S3	Rb1	$S1^{11}$	83.18(4)	S2	Sr1	$S2^{2}$	164.94(3)
S3	Rb1	$S2^{12}$	123.90(4)	$S1^{6}$	Sr2	Br1	72.10(3)
$S3^{10}$	Rb1	$S2^{13}$	123.90(4)	$S1^{7}$	Sr2	Br1	138.59(3)
$S3^{10}$	Rb1	$S2^{12}$	65.13(3)	$S1^{6}$	Sr2	$S1^{7}$	147.26(2)
S3	Rb1	$S2^{13}$	65.13(3)	$S1^{6}$	Sr2	S2	91.55(4)
S3	Rb1	$S3^{10}$	128.05(6)	$S1^{7}$	Sr2	S2	71.29(4)
$S1^{3}$	Sr1	$Br1^{1}$	126.89(3)	$S1^{6}$	Sr2	$S2^{5}$	89.89(4)
$S1^{4}$	Sr1	$Br1^{1}$	68.34(3)	$S1^{6}$	Sr2	$S3^{7}$	150.56(4)
S1	Sr1	$Br1^{1}$	126.89(3)	$S1^{7}$	Sr2	$S3^{7}$	60.00(4)
$S1^{2}$	Sr1	$Br1^{1}$	68.34(3)	$S1^{7}$	Sr2	$S3^{6}$	88.57(3)
$S1^{4}$	Sr1	$S1^{3}$	164.22(3)	$S1^{6}$	Sr2	$S3^{6}$	59.30(4)
$S1^{2}$	Sr1	$S1^{4}$	70.42(5)	S2	Sr2	Br1	138.12(3)
$S1^{4}$	Sr1	S1	109.39(4)	$S2^{5}$	Sr2	Br1	70.89(3)
$S1^{2}$	Sr1	S1	164.22(3)	$S2^{5}$	Sr2	$S1^{7}$	91.62(4)
$S1^{2}$	Sr1	$S1^{3}$	109.39(4)	$S2^{5}$	Sr2	S2	149.343(17)
S1	Sr1	$S1^{3}$	66.26(5)	S2	Sr2	$S3^{6}$	72.72(3)
$S1^{2}$	Sr1	$S2^{4}$	101.36(4)	$S2^{5}$	Sr2	$S3^{6}$	81.85(4)
$S1^{4}$	Sr1	$S2^{2}$	101.36(4)	S2	Sr2	$S3^{7}$	114.34(3)
$S1^{4}$	Sr1	$S2^{4}$	58.22(4)	$S2^{5}$	Sr2	$S3^{7}$	75.08(4)

S3	Sr2	Br1	81.37(3)	S3	Sr2	S3^{7}	82.84(2)
S3^{7}	Sr2	Br1	79.03(3)	S3	Sr2	S3^{6}	129.42(5)
S3	Sr2	S1^{6}	98.16(4)	S3^{7}	Sr2	S3^{6}	139.68(4)
S3	Sr2	S1^{7}	98.11(4)	S1	B1	S2	116.0(3)
S3	Sr2	S2	62.63(3)	S3	B1	S1	120.1(3)
S3	Sr2	S2^{5}	147.17(4)	S3	B1	S2	123.9(3)

Symmetry transformations used to generate equivalent atoms:

^{1}3/2-X,3/2-Y,1/2+Z; ^{2}2-X,1-Y,1/2+Z; ^{3}2-X,+Y,+Z; ^{4}+X,1-Y,1/2+Z; ^{5}3/2-X,3/2-Y,-1/2+Z; ^{6}3/2-X,1/2+Y,+Z; ^{7}+X,1-Y,-1/2+Z; ^{8}1-X,1-Y,-1/2+Z; ^{9}1-X,1-Y,1/2+Z; ^{10}1-X,+Y,+Z; ^{11}3/2-X,1/2-Y,-1/2+Z; ^{12}-1/2+X,-1/2+Y,+Z; ^{13}3/2-X,-1/2+Y,+Z; ^{14}-1/2+X,1/2-Y,-1/2+Z; ^{15}2-X,1-Y,-1/2+Z; ^{16}3/2-X,1/2-Y,1/2+Z; ^{17}1/2+X,1/2+Y,+Z

Table S8. The calculated band gaps (in GGA), birefringence, the largest SHG coefficients of $Sr_3B_2S_6$ and $[RbSr_3X][(BS_3)_2]$ (X = Cl, Br).

Formula	Symmetry	Band gap	Birefringence	SHG tensor
$Sr_3B_2S_6$	CS	2.30 eV	0.197 at 1064nm	/
$[RbSr_3Cl][(BS_3)_2]$	CS	2.60 eV	0.136 at 1064nm	/
$[RbSr_3Br][(BS_3)_2]$	NCS	2.59 eV	0.138 at 1064nm	1.77 pm/V

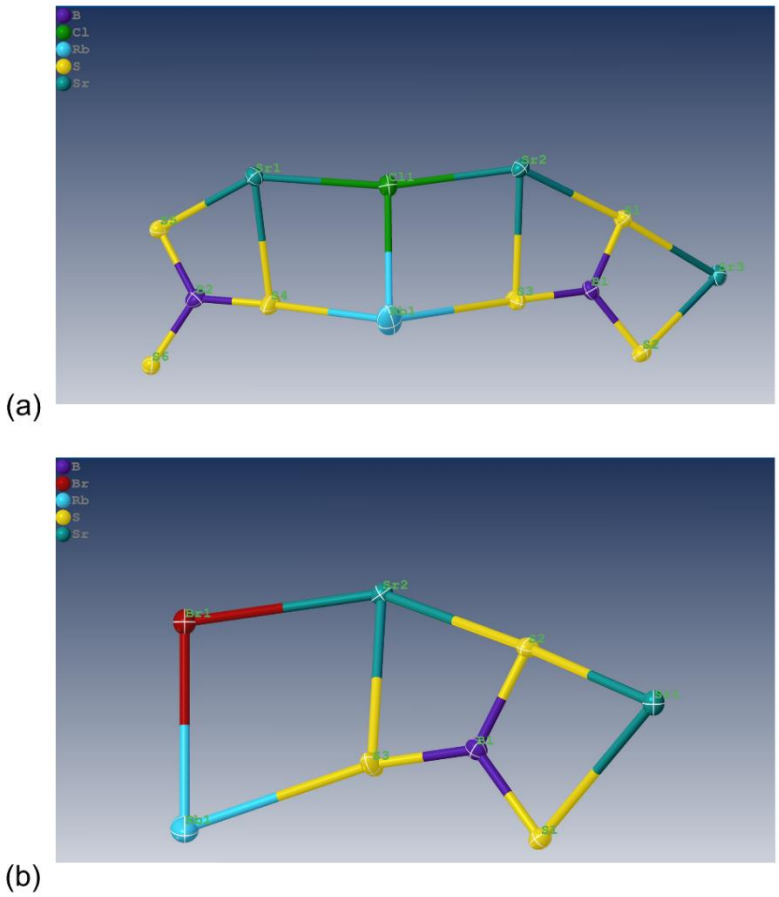

Figure S1. Ellipsoids styles of $[RbSr_3X][(BS_3)_2]$ (X = Cl, Br) structures (using Olex2). a) Ellipsoids styles of $[RbSr_3Cl][(BS_3)_2]$; b) Ellipsoids styles of $[RbSr_3Br][(BS_3)_2]$.

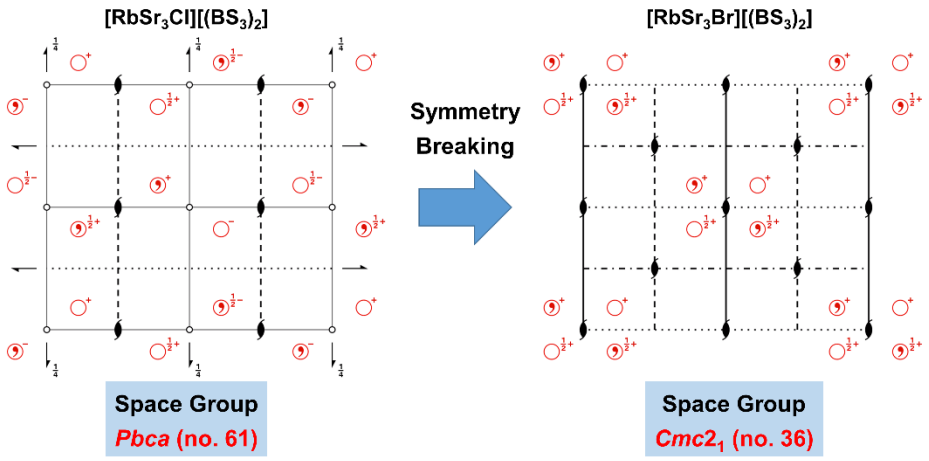

Figure S2. Spatial symmetry operation change from CS $[RbSr_3Cl][(BS_3)_2]$ [high symmetry *Pbca* (no. 61)] to NCS $[RbSr_3Br][(BS_3)_2]$ [low symmetry $Cmc2_1$ (no. 36)].

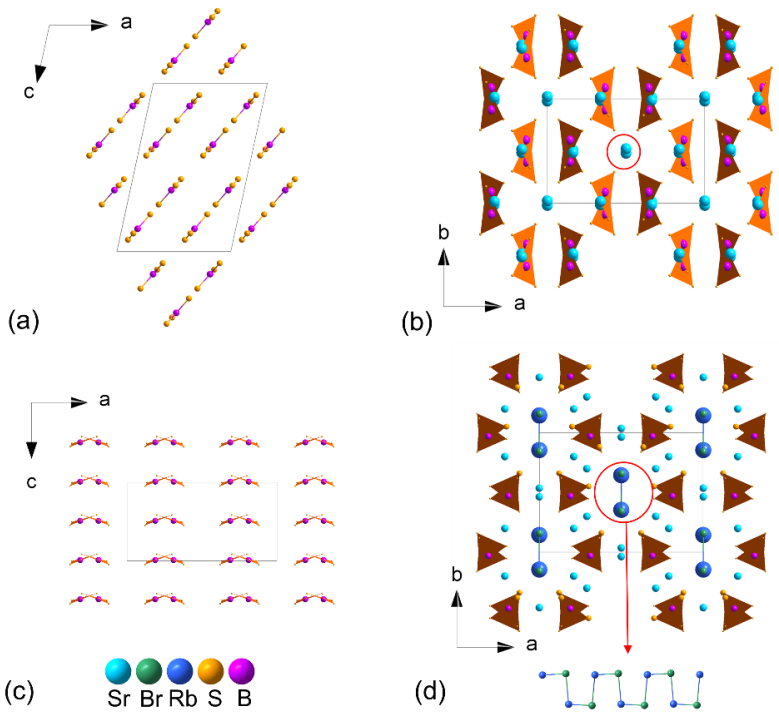

Figure S3. The structural comparison between $Sr_3B_2S_6$ and title compounds (taking $[RbSr_3Br][(BS_3)_2]$ as an example). a and b) The arrangement of $[BS_3]$ units and structure of $Sr_3B_2S_6$; c and d) The arrangement of $[BS_3]$ units and structure of $[RbSr_3Br][(BS_3)_2]$.

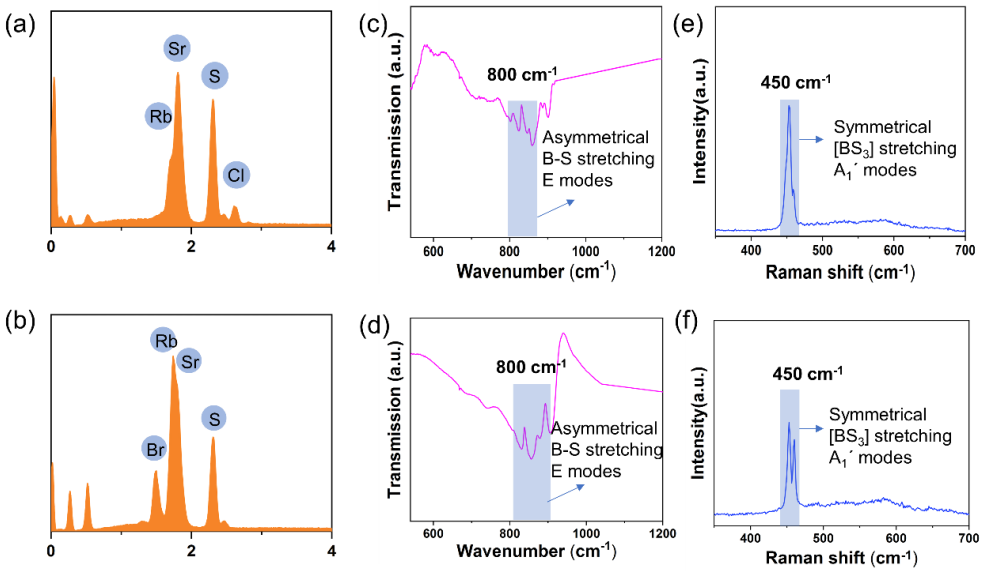

Figure S4. The experimental measurements of $[RbSr_3X][(BS_3)_2]$ (X = Cl, Br). a and b) The Energy dispersive X-ray spectroscopy; c and d) The Raman spectra; e and f) The IR absorption spectra.

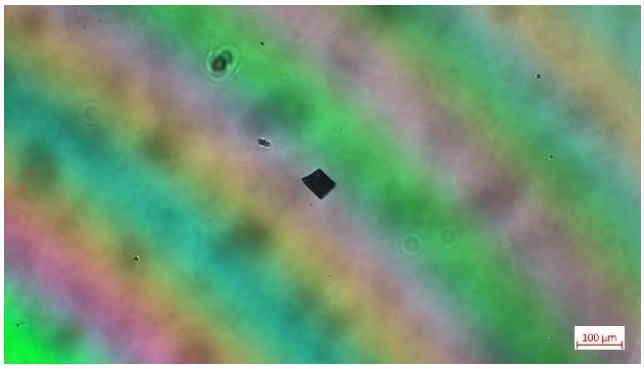

Figure S5. The birefringence measurement of $[RbSr_3Cl][(BS_3)_2]$.

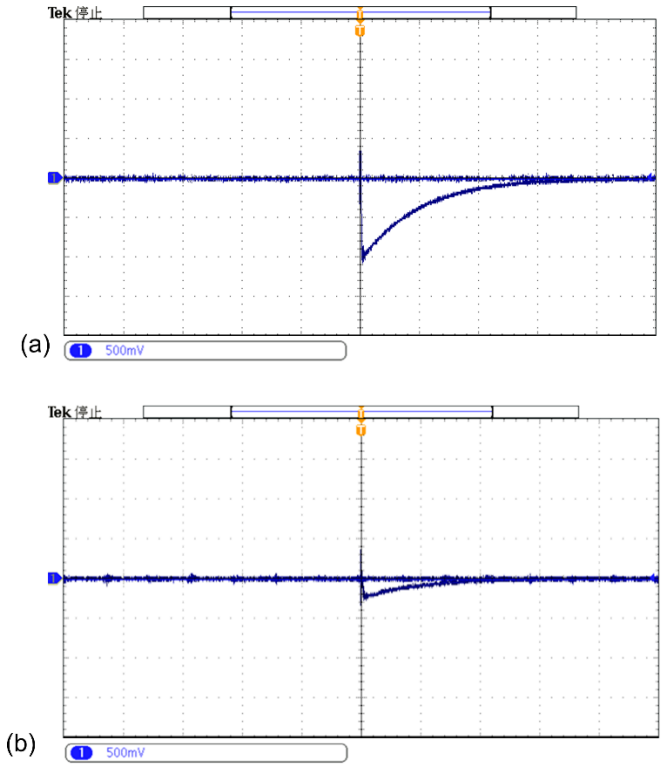

Figure S6. The SHG measurement of $[RbSr_3Br][(BS_3)_2]$. a) The signal strength of AGS; b) The signal strength of $[RbSr_3Br][(BS_3)_2]$.

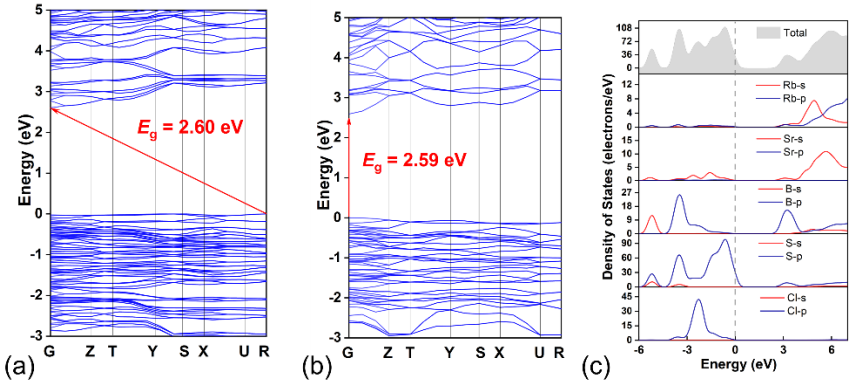

Figure S7. The calculated results of $[RbSr_3X][(BS_3)_2]$ (X = Cl, Br). a and b) Band structures of $[RbSr_3X][(BS_3)_2]$ (X = Cl, Br); c) Density of states of $[RbSr_3Cl][(BS_3)_2]$

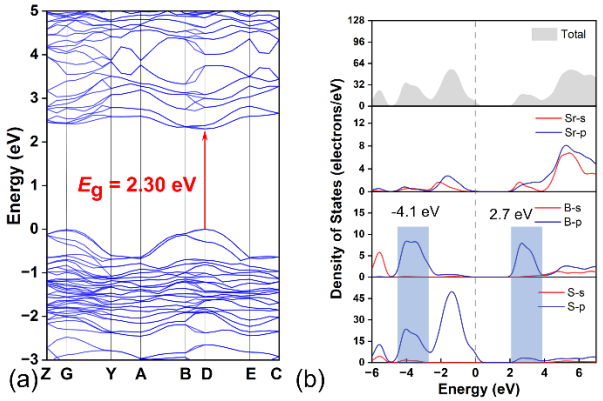

Figure S8. The calculated results of $Sr_3B_2S_6$. a) Band structure; b) Density of states.

Reference

1. B. Macías, I. García, M. V. Villa, J. Borrás, A. Castiñeiras, F. Sanz, *Z. Anorg. Allg. Chem.*, 2003, **629**, 255-260.
2. G. Kortüm, in *Reflectance Spectroscopy: Principles, Methods, Applications* (Ed.: G. Kortüm), Springer Berlin Heidelberg, Berlin, Heidelberg, 1969, pp. 170-216.
3. J. Guo, A. Tudi, S. Han, Z. Yang, S. Pan, *Angew. Chem. Int. Ed.*, 2019, **58**, 17675-17678.
4. G. Peng, C. Lin, D. Zhao, L. Cao, H. Fan, K. Chen, N. Ye, *Chem. Commun.*, 2019, **55**, 11139-11142.
5. C. Wu, X. Jiang, L. Lin, Z. Lin, Z. Huang, M. G. Humphrey, C. Zhang, *Chem. Mater.*, 2020, **32**, 6906-6915.
6. S. K. Kurtz, T. T. Perry, *J. Appl. Phys.*, 1968, **39**, 3798-3813.
7. P. Geerlings, F. De Proft, W. Langenaeker, *Chem. Rev.*, 2003, **103**, 1793-1874.
8. J. P. Perdew, K. Burke, M. Ernzerhof, *Phys. Rev. Lett.*, 1996, **77**, 3865-3868.
9. A. M. Rappe, K. M. Rabe, E. Kaxiras, J. D. Joannopoulos, *Phys. Rev. B*, 1990, **41**, 1227-1230.
10. J. S. Lin, A. Qteish, M. C. Payne, V. Heine, *Phys. Rev. B*, 1993, **47**, 4174-4180.
11. S. J. Clark, M. D. Segall, C. J. Pickard, P. J. Hasnip, M. I. J. Probert, K. Refson, M. C. Payne, *Z. Kristallogr. - Cryst. Mater.*, 2005, **220**, 567-570.
12. J. Heyd, G. E. Scuseria, M. Ernzerhof, *J. Chem. Phys.*, 2003, **118**, 8207-8215.
13. J. Lin, M.. Lee, Z. Liu, C. Chen, C. J. Pickard, *Phys. Rev. B*, 1999, **60**, 13380-13389.
14. B. Lei, Z. Yang, S. Pan, *Chem. Commun.*, 2017, **53**, 2818-2821.